

# Transition to turbulent convection in a fluid layer heated from below at moderate aspect ratio

By T. HARTLEP<sup>1</sup>†, A. TILGNER<sup>1</sup> AND F. H. BUSSE<sup>2</sup>

<sup>1</sup>Institute of Geophysics, University of Göttingen, Friedrich-Hund-Platz 1, 37077 Göttingen, Germany

<sup>2</sup>Institute of Physics, University of Bayreuth, 95440 Bayreuth, Germany

(Received 2 December 2004 and in revised form 15 June 2005)

Numerical simulations of Rayleigh–Bénard convection in a fluid layer heated from below between two rigid horizontal boundaries have been performed for Rayleigh numbers  $Ra$  up to  $10^7$ , Prandtl numbers in the range between 0.7 and 60 and for aspect ratios  $\Gamma$  up to 20. Periodic boundary conditions in the horizontal plane have been used. To a considerable extent, the evolution towards turbulent convection at high values of  $Ra$  is governed by processes exhibited by instabilities of steady or time periodic forms of convection at lower Rayleigh numbers. With increasing  $Ra$ , the properties of convection are increasingly determined by the thermal boundary layers. The role of mean flows which may be symmetric or antisymmetric with respect to the mid-plane of the layer is emphasized.

---

## 1. Introduction

Thermal convection in fluid layers heated from below has long been a preferred subject for the study of fluid turbulence under physically realistic conditions. The property that turbulent eddies can be observed in their evolution in time within the laboratory frame of reference instead of being swept away by a mean flow, together with the fact that the temperature field offers convenient additional opportunities for visualizations and measurements, has made thermal convection an attractive subject from the experimental point of view. The localized nature of convection flows also offers many advantages from the theoretical point of view. The most important properties of turbulent convection can be investigated by restricting the numerical analysis to relatively small horizontal periodicity intervals or boxes with aspect ratio of the order unity. Much attention has thus been devoted in recent years to the goal of reaching high Rayleigh numbers  $Ra$  in experiments as well as in numerical simulations in order to gain an understanding of the asymptotic regime of large  $Ra$ . It is expected that this regime is not only important for applications to convection in the atmosphere and in stars, but that it will also provide general insights into the nature of turbulent transport processes.

Some features of turbulent convection, however, cannot be described adequately when the analysis is restricted to low-aspect-ratio boxes. The fact that in experiments hot rising and cold descending plumes occur at sidewalls is likely to yield a Nusselt–Rayleigh number relationship different from that obtained in horizontally extended layers where plumes occur predominantly in the interior of the layer. There is also

† Present address: Centre for Turbulence Research, Stanford University, Building 500, Stanford, CA 94305-3035, USA.

the question of whether large scale mean flows can be generated by convection, as has been suggested by Krishnamurti & Howard (1981). The spontaneously selected size of circulation cells in turbulent convection is known to increase with  $Ra$ , at least in the case of moderate Prandtl numbers. The nature of the network of quasi-stationary cells is not well understood, even though it appears to persist to asymptotically high Rayleigh numbers as the observations of mesoscale convection in the atmosphere and of solar granulation tend to suggest. Questions such as these have motivated the numerical study presented in this paper.

By using quadratic periodicity intervals in the horizontal plane with typical aspect ratios up to  $\Gamma = 10$ , we hope to gain some understanding of the dependence of properties on the aspect ratio and to provide a basis for extrapolations to the case of infinitely extended layers. In fact,  $\Gamma = 10$  may not be sufficient for this purpose and  $\Gamma = 20$  has been used for this reason in some cases. Of course, the limits of available computer capacity restrict the regime of accessible Rayleigh numbers the more the higher the aspect ratio is chosen. While in most cases numerical simulations have been carried out up to  $Ra = 10^6$ , in several instances  $Ra = 10^7$  has been reached.

The paper is organized as follows. After the formulation of the mathematical problem and a brief introduction to the numerical methods in §2, an overview of the convection structures in dependence on the Prandtl number is given in §3. Here, and in the following sections, we shall refer frequently to earlier work in which the evolution of convection patterns through sequences of bifurcations from rolls to three-dimensional steady and time-dependent forms of flow has been investigated. In fact, many of the characteristic features of turbulent convection found in the numerical simulations can be traced to properties of convection introduced by bifurcations. Examples of this kind are exhibited by the mean flow properties discussed in §4 and similar relationships can be found in some aspects of the convective heat transport which is described in §5. Concluding remarks are made in §6.

## 2. Mathematical formulation of the problem

We consider an infinitely extended horizontal fluid layer of height  $d$  between two rigid plates of which the upper one is kept at the temperature  $T_0$  and the lower one at the temperature  $T_0 + \Delta T$ . A Cartesian coordinate system will be used with the acceleration due to gravity  $g$  acting in the negative  $z$ -direction. Periodic boundary conditions are imposed in  $x$ - and  $y$ -directions with periodicity lengths  $l_x$  and  $l_y$ . The aspect ratio  $\Gamma$  is defined as  $\Gamma = l_x/d = l_y/d$ . Using  $d$ ,  $d^2/\kappa$ ,  $\Delta T$  as units of length, time and temperature, respectively, where  $\kappa$  is thermal diffusivity, we obtain non-dimensional equations for the velocity field  $\mathbf{v}(\mathbf{r}, t)$  and the temperature  $T(\mathbf{r}, t)$ . Since we employ the Boussinesq approximation, two dimensionless control parameters enter the equations: the Rayleigh number  $Ra = g\alpha d^3 \Delta T / (\kappa \nu)$  and the Prandtl number  $Pr = \nu/\kappa$ , where  $\nu$  is the kinematic viscosity of the fluid and  $\alpha$  is its coefficient of thermal expansion. When the fluid is at rest, the (dimensionless) temperature depends only on  $z$  and varies as  $T(z=0) - z$ . In the general case, it is convenient to specify the temperature through the deviation  $\Theta$  from the static profile:  $T(\mathbf{r}, t) = \Theta(\mathbf{r}, t) + T(z=0) - z$ . The equations of motion for  $\mathbf{v}(\mathbf{r}, t)$  and  $\Theta(\mathbf{r}, t)$  are:

$$\partial_t \mathbf{v} + (\mathbf{v} \cdot \nabla) \mathbf{v} = -\nabla \pi + Pr \nabla^2 \mathbf{v} + Ra Pr \Theta \hat{z}, \quad (2.1)$$

$$\nabla \cdot \mathbf{v} = 0, \quad (2.2)$$

$$\partial_t \Theta + \mathbf{v} \cdot \nabla \Theta - \mathbf{v} \cdot \hat{z} = \nabla^2 \Theta, \quad (2.3)$$

where  $\hat{z}$  is the unit vector in  $z$ -direction and terms that can be written as gradients have been combined into  $\nabla\pi$ . The velocity field can be represented uniquely by a poloidal scalar  $\phi(\mathbf{r}, t)$ , a toroidal scalar  $\psi(\mathbf{r}, t)$  and a mean flow  $\mathbf{U}(z, t)$ ,

$$\mathbf{v} = \nabla \times \nabla \times \phi \hat{z} + \nabla \times \psi \hat{z} + \mathbf{U}, \quad (2.4)$$

where  $\phi$  and  $\psi$  are bounded functions with vanishing average over the  $(x, y)$ -plane. The boundary conditions are given by

$$\Theta = 0, \quad \mathbf{v} = 0 \quad \text{at } z = 0, 1. \quad (2.5)$$

Equations of motion for  $\phi$ ,  $\psi$  and  $\mathbf{U}$  are obtained from the  $z$ -component of the curl of the curl of (2.1), the  $z$ -component of the curl of (2.1), and the average over horizontal planes of (2.1), respectively,

$$\nabla^4 \Delta_2 \phi - \Delta_2 \Theta = (\hat{z} \cdot \nabla \times (\nabla \times (\mathbf{v} \cdot \nabla) \mathbf{v}) + \partial_t \nabla^2 \Delta_2 \phi) Pr^{-1}, \quad (2.6)$$

$$\nabla^2 \Delta_2 \psi = (\hat{z} \cdot \nabla \times (\mathbf{v} \cdot \nabla) \mathbf{v} + \partial_t \Delta_2 \psi) Pr^{-1}, \quad (2.7)$$

$$(\partial_{zz}^2 - Pr^{-1} \partial_t) \mathbf{U} = -\partial_z \Delta_2 \Phi (\nabla_2 \partial_z \Phi + \nabla \Psi \times \hat{z}) / Pr, \quad (2.8)$$

where  $\nabla_2$  is given by  $\nabla_2 = \nabla - \hat{z} \hat{z} \cdot \nabla$  and  $\Delta_2$  denotes the horizontal Laplacian,  $\Delta_2 = \partial_{xx}^2 + \partial_{yy}^2$ .

A spectral method (Moser, Moin & Leonard 1983; Kerr 1996; Hartlep & Tilgner 2003) is used to solve (2.3) and (2.6) numerically. Space is discretized with Chebychev polynomials in the  $z$ -direction and with Fourier modes in the  $x$ - and  $y$ -directions. Dealiasing with the 2/3-rule is implemented. The time-marching procedure is a second-order Adams–Bashforth scheme for the advection and buoyancy terms coupled to a Crank–Nicolson scheme for the diffusive terms. An adaptive time step is used to speed up the transients. All computations have been started from random noise as initial conditions, and have been run for several tens of the convection time scale  $\tau = (2E_{kin})^{-1/2}$ , with  $E_{kin}$  being the average kinetic energy density. Spatial resolution was up to 65 Chebychev polynomials and  $512^2$  grid points in horizontal planes. The code has been validated by comparing the results with those obtained with a completely independent Galerkin method (Clever & Busse 1987, 1994).

### 3. Evolution of convection patterns

Rayleigh–Bénard convection is known for its rich variety of patterns which appear to persist even into the regime of fully developed turbulence, as the examples of cloud patterns in the atmosphere and of solar granulation indicate. Many of the characteristic patterns are associated with special boundary conditions or deviations from the Boussinesq approximation which will not be considered in this paper. For numerical simulations of turbulent convection in the presence of strongly temperature-dependent viscosity at infinite Prandtl number see Balachandar, Yuen & Reuteler (1996). Here, we shall focus first on patterns in the case of  $Pr = 0.7$  and then proceed to moderately high Prandtl numbers in the range of  $7 \leq Pr \leq 60$ .

#### 3.1. Pattern evolution for Prandtl numbers of the order unity

The characteristic changes occurring in the spatio-temporal structure of convection for  $Pr \approx 1$  are evident from figures 1 and 2. The onset of convection occurs in the form of straight rolls with a wavenumber  $q$  close to the critical value 3.116. In the present case of discrete wavenumbers determined by the finite periodicity interval  $\Gamma = 10$ ,  $q = 3.142$  was found. In quantitative agreement with experimental observations (Willis, Deardorff & Somerville 1972), a rapidly decreasing wavenumber with increasing

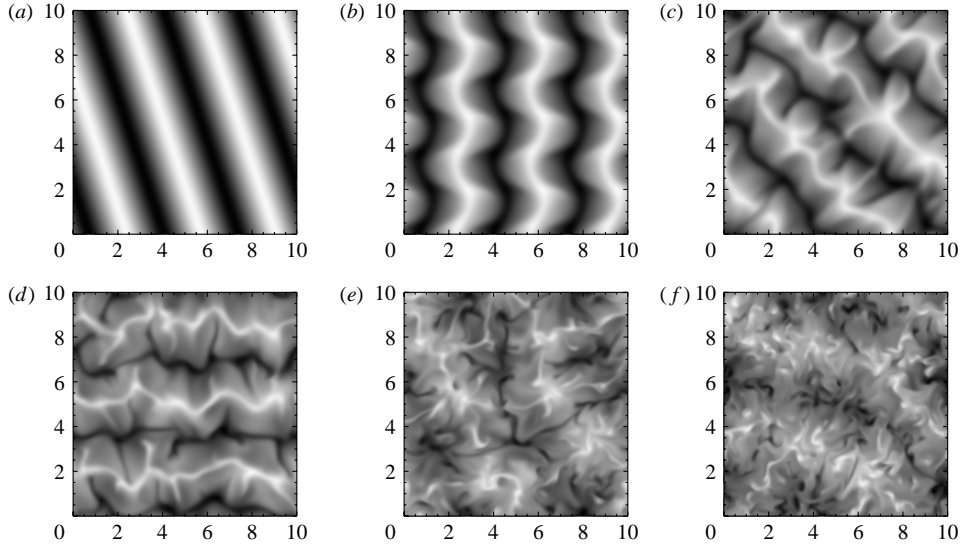


FIGURE 1. Snapshots of the temperature in the mid-plane ( $z=0.5$ ) for  $Pr=0.7$ ,  $\Gamma=10$  and (a)  $Ra=4 \times 10^3$ , (b)  $8 \times 10^3$ , (c)  $1.6 \times 10^4$ , (d)  $3.2 \times 10^4$ , (e)  $10^5$  and (f)  $2.5 \times 10^5$ . Cold and hot fluid is shown in white and black, respectively.

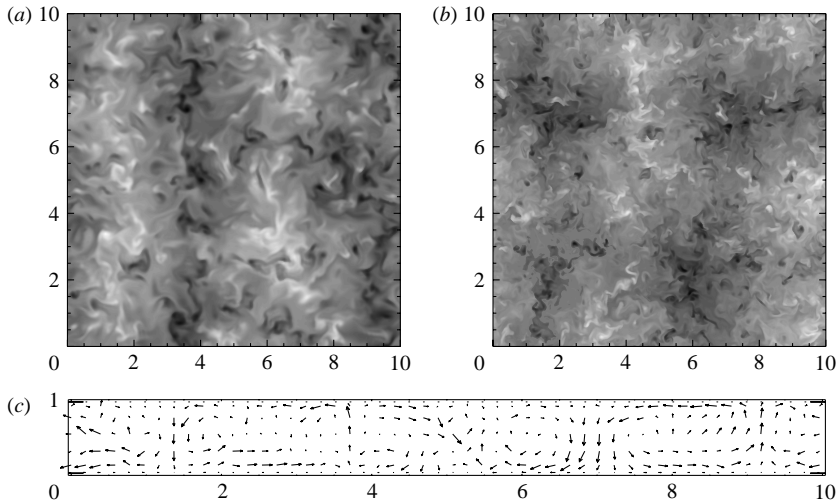


FIGURE 2. Mid-plane temperatures for (a)  $Ra=10^6$  and (b)  $Ra=10^7$ , and, (c) for the case of  $Ra=10^6$ , the corresponding velocity field in the  $(x, z)$ -plane at  $y=1.75$ . In both cases, a Prandtl number of  $Pr=0.7$  and an aspect ratio of  $\Gamma=10$  was used.

$Ra$  can be observed when simulations are started with random initial conditions. Accordingly, rolls with  $q=2.0$  are seen in figure 1(a). The oscillatory instability sets in at about  $Ra=5.5 \times 10^3$  for this wavenumber (Clever & Busse 1974) and a pattern of sinusoidal displacements propagating along the axis of the rolls is realized as indicated in figure 1(b). As their amplitude increases, these waves become unstable to tertiary instabilities (Clever & Busse 1987) and a transition to a chaotic regime of convection occurs. In spite of the increasing complexity of the small-scale motions, a large scale arrangement of basic rolls with a wavelength of half the aspect ratio

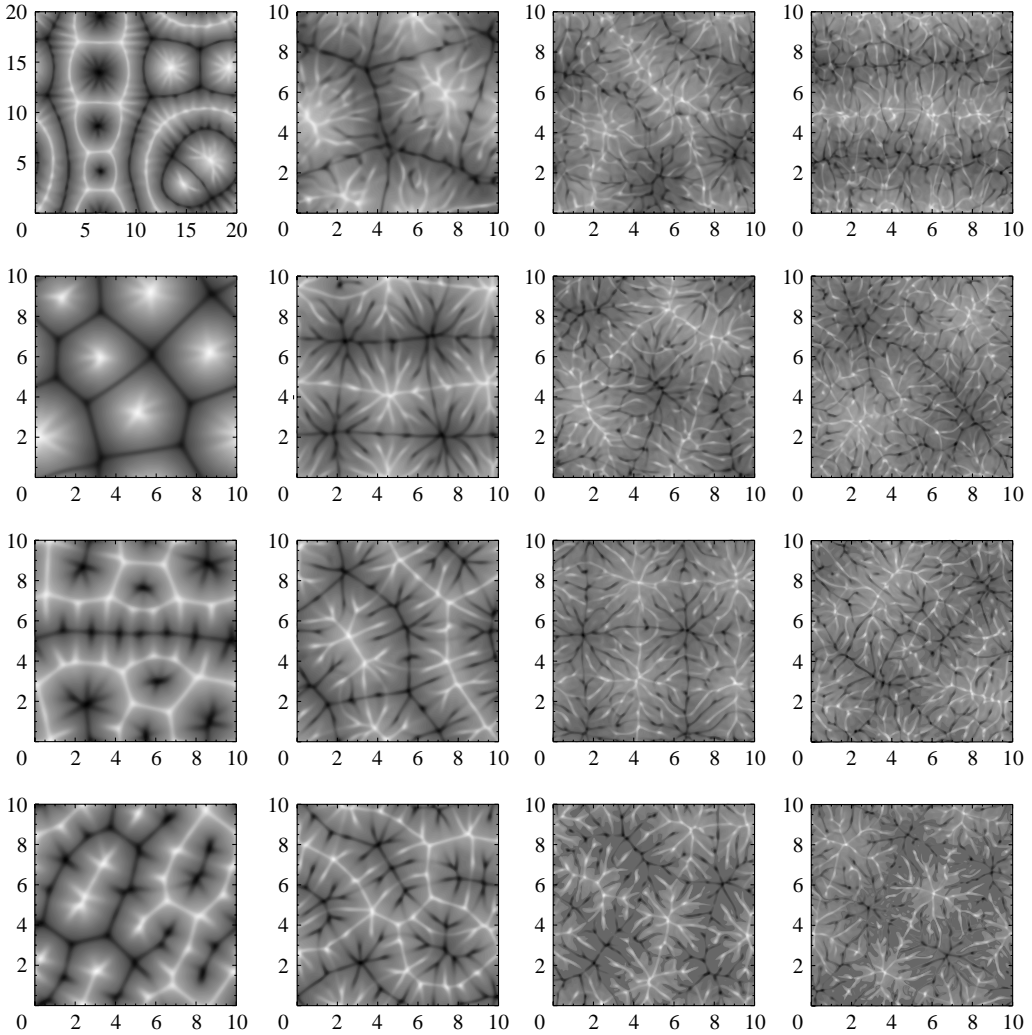


FIGURE 3. Horizontal distribution of the instantaneous vertically averaged temperature for Rayleigh numbers  $Ra = 3.2 \times 10^4$ ,  $10^5$ ,  $5 \times 10^5$  and  $10^6$  (left to right) and Prandtl numbers  $Pr = 7$ , 15, 30 and 60 (top to bottom). The aspect ratio is  $\Gamma = 10$  for all simulations except for the case  $Ra = 3.2 \times 10^3$ ,  $Pr = 7$  (top left), in which  $\Gamma = 20$ .

can still be seen most of the time. Sometimes the arrangement assumes the form of square cells as in the case of  $Ra = 10^7$  in figure 2. The vertical cross-section shown in figure 2(c) demonstrates that the circulation corresponding to the horizontal pattern does indeed pass through the entire depth of the layer. An analysis of the average size of these large-scale structures and its dependence on  $Ra$  and  $Pr$  can be found in Hartlep, Tilgner & Busse (2003).

### 3.2. Pattern evolution at moderately high Prandtl numbers

In figure 3, the evolution of convection structures with increasing Rayleigh number is shown for four different Prandtl numbers between 7 and 60. While convection starts in the form of rolls at the critical value  $Ra = 1708$ , various instabilities have occurred by the time the lowest value of  $Ra$  used for the figure has been reached. For a detailed

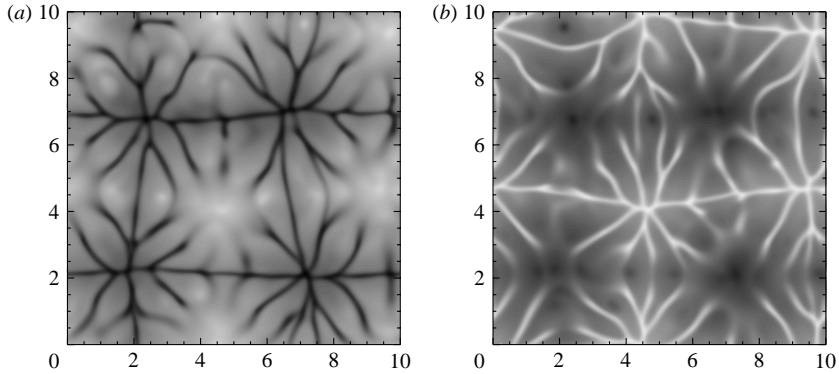


FIGURE 4. Snapshots of the temperature field in two horizontal planes, (a)  $z=0.18$  and (b)  $z=0.82$ , for a simulation with  $Ra = 10^5$ ,  $Pr = 15$  and  $\Gamma = 10$ .

discussion of these instabilities in the relevant range of Prandtl numbers, see Bolton, Busse & Clever (1986). It is surprising to see convection in the form of polygonal cells in the cases of  $Pr = 7$  and  $Pr = 15$ , since the occurrence of hexagonal cells is usually associated with deviations from the Boussinesq approximation which are absent in our computations. Moreover, cells with both signs of vertical motion in the cell centre can be seen in the case  $Pr = 7$ . That only cells with descending motion in the centre are visible in the plot for  $Pr = 15$  is caused by the small periodicity interval. The four-times larger horizontal area used in the case  $Pr = 7$  appears to be required in order to provide sufficient space for coexisting cells of both signs. Note that a convection roll separates the two types of cells, just as in the case of the experimental observations of Assenheimer & Steinberg (1996). This appearance of coexistent types of convection structures is in agreement with the property that there exists an intermediate range of Rayleigh numbers where hexagonal convection cells of both signs as well as rolls represent stable steady solutions (Clever & Busse 1996).

For  $Pr = 60$ , the tendency towards polygonal convection cells is no longer clearly evident, and only the bimodal structure of convection is visible which is caused by the superposition of smaller cross-rolls onto the basic rolls. This type of convection has been studied theoretically (Busse 1967; Frick, Busse & Clever 1983) as well as experimentally (Busse & Whitehead 1971) and is well understood.

While the convection flows are approximately steady for  $Ra = 3.2 \times 10^4$ , a time dependence, especially of the small-scale structures, develops on the way to the next higher value of  $Ra$ . The typical patterns found at this and even higher values of  $Ra$  have been called spoke patterns (Busse & Whitehead 1974) because the convection structure appears to be governed by central plumes which are fed by spoke like ridges of hot and cold fluid in the respective boundary layers. The fact that the ‘spokes’ do not penetrate through the entire layer is evident from patterns close to the upper and lower boundaries shown in figure 4 for the particular case of  $Pr = 15$  and  $Ra = 10^5$ .

#### 4. Mean flows generated by convection

There are several mechanisms through which laminar convection may generate mean flows, i.e. flows without an  $(x, y)$ -dependence which are described by the component  $U$  of the velocity field (2.4). At Prandtl numbers of the order unity, a mean flow symmetric with respect to  $z = 0.5$  is generated along the axis of convection rolls after the oscillatory instability has set in and wavy distortions travelling along the

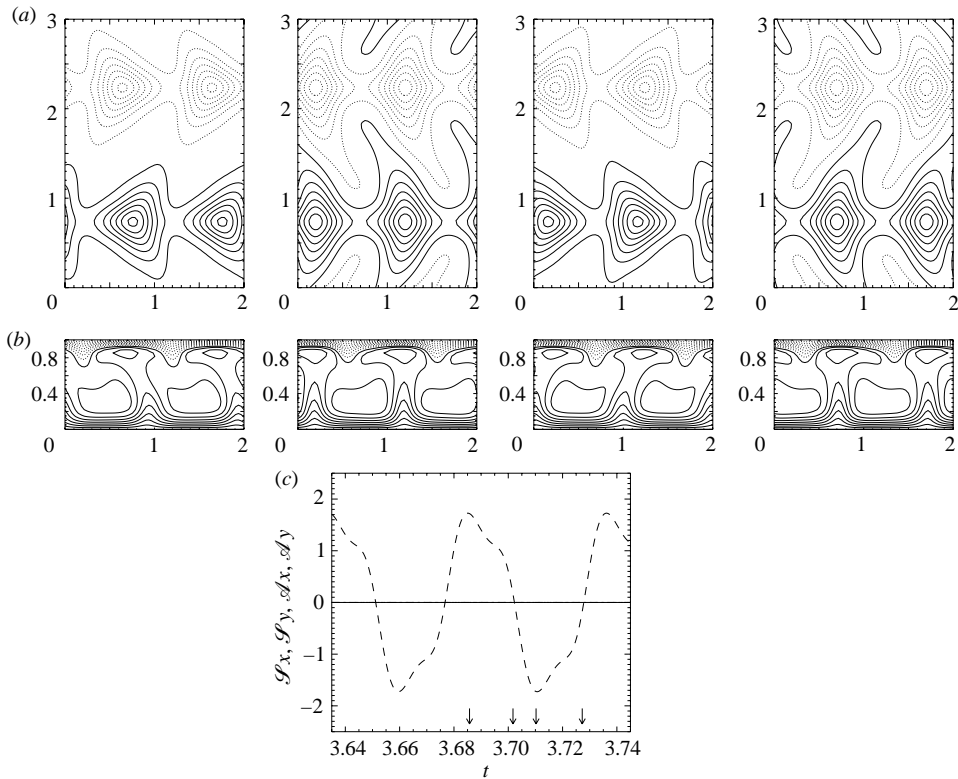


FIGURE 5. (a) Contour plots of vertical velocity in the mid-plane and (b) temperature in the  $(x, z)$ -plane at  $y=1$  at four different times as indicated by the arrows in (c) (from left to right) in a simulation with  $Ra = 6.4 \times 10^4$ ,  $Pr = 7$ ,  $\Gamma_x = l_x/d = 2$ ,  $\Gamma_y = l_y/d = 3$ . Solid and broken lines indicate positive and negative values, respectively. (c) also shows time series of the mean flow with solid and dotted lines denoting the symmetric parts  $\mathcal{S}_i = \langle \int_0^1 U_i dz \rangle_{x,y}$  ( $i = x, y$ ), and with dashed and dash-dotted lines denoting the antisymmetric parts  $\mathcal{A}_i = \langle \int_0^1 2(1 - 2z)U_i dz \rangle_{x,y}$  ( $i = x, y$ ), respectively. Since solid, dotted, and dash-dotted lines coincide with zero, only  $\mathcal{A}_x$  exhibits a finite value.

rolls have appeared (Clever & Busse 1989). At higher Prandtl numbers, a steady mean flow which is also symmetric with respect to  $z = 0.5$  is found after the instability of rolls in the form of travelling blob oscillations has set in (Clever & Busse 1995). Travelling blob oscillations are rarely seen, however, in experiments or numerical simulations. An oscillatory mean flow which is antisymmetric with respect to  $z = 0.5$  is generated by the wavy oscillatory instability of bimodal convection (Clever & Busse 1994). The secondary small, wavelength rolls which are superimposed at a right angle onto the basic rolls tilt back and forth in the direction of the axis of the basic rolls. Because of the periodic tilt, a Reynolds stress is generated with the same period. The tilt is clearly evident in the plots of figure 5 which also shows the mean flow generated by this mechanism.

According to this discussion symmetric mean flows along the basic rolls must be expected for Prandtl numbers of the order unity or less, while an antisymmetric oscillating mean flow should typically be seen at higher Prandtl numbers. This expectation is borne out to some extent by the results of the numerical simulations. In figure 6(a), the Rayleigh number is sufficiently low such that a regular convection pattern is still realized, as is also evident from the corresponding plot of figure 1. Besides the expected

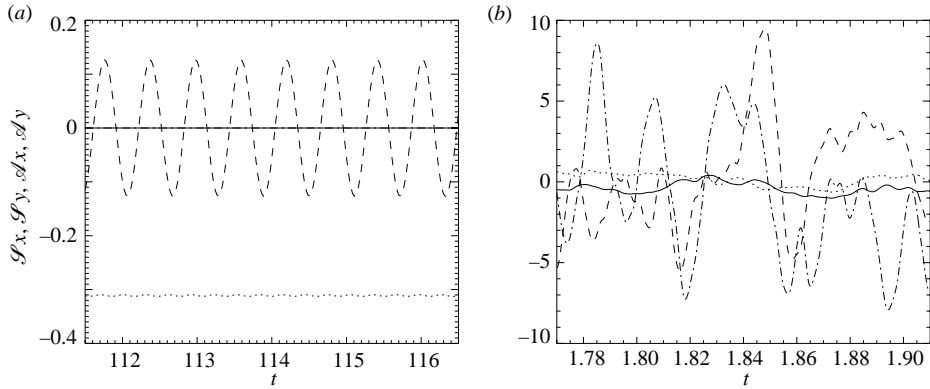


FIGURE 6. Time series of mean flow components for (a)  $Ra = 8 \times 10^3$  and (b)  $Ra = 10^6$ , both for  $Pr = 0.7$ ,  $\Gamma = 10$ . As in figure 5, solid and dotted lines indicate symmetric parts, dashed and dash-dotted lines indicate antisymmetric parts of the mean flow velocities  $U_x$  and  $U_y$ , respectively.

steady symmetric mean flow along the roll axis, there also exists an oscillatory anti-symmetric mean flow with a period twice as long as the period of the wave travelling along the rolls. The antisymmetric mean flow is obviously caused by the onset of the asymmetric instability of travelling-wave convection (Clever & Busse 1987). This instability introduces a tilt in the streets of rising and descending motion and thus creates a Reynolds stress. Since the frequency  $\omega_2$  of the asymmetric instability tends to phase lock with the symmetric oscillation (frequency  $\omega_1$ ) such that  $\omega_2 = \omega_1/2$ , the observed period of the antisymmetric oscillatory mean flow must be expected. It should be mentioned that the transition from symmetric oscillatory convection to asymmetric oscillatory convection was first observed in the numerical simulations of Lipps (1976).

As the Rayleigh number is increased and a turbulent state of convection is realized, the antisymmetric component of the mean flow increases relative to the symmetric one, as is evident from the time series of figure 6. It is also evident from this figure that symmetric as well as antisymmetric components of the mean flow tend to vanish in the time average in the turbulent case.

In the case of larger Prandtl numbers, the antisymmetric mean flow appears to dominate in the entire Rayleigh number regime that has been investigated. Although the large-scale convection pattern at  $Ra = 3.2 \times 10^4$  is nearly steady, as shown in the upper left plot of figure 3, the antisymmetric mean flow exhibits a rather chaotic time dependence with strong oscillations with frequencies  $\omega$  of the order 70 (based on the thermal time scale). This property indicates the origin of this mean flow from the small wavelength component of convection which is also strongly time dependent. The typical frequency  $\omega$  of the order  $10^2$  agrees with that found for the wavy oscillatory instability of bimodal convection at comparable values of  $Ra$  (Clever & Busse 1994). The frequency is expected to increase in proportion to  $Ra^{2/3}$ . An increase of the characteristic frequency, albeit a smaller one, is indeed found in the numerical simulations. Except for this change in the frequency spectrum, the results at  $Ra = 10^6$  are remarkably similar to those at  $Ra = 3.2 \times 10^4$ , at least as far as the mean flow properties are concerned.

The results for the dependence of the mean flow energies on the Rayleigh number are summarized in figure 7 for the cases  $Pr = 0.7$  and  $Pr = 7$ . It is remarkable how little the distribution of the kinetic energy of convection on the various components

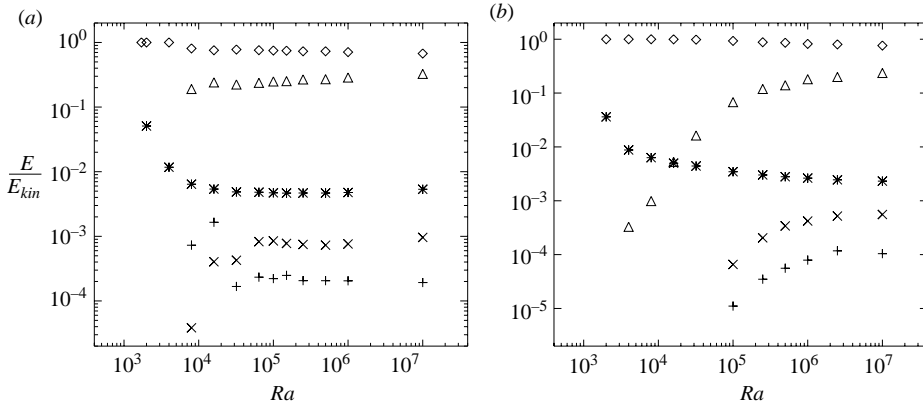


FIGURE 7. Rayleigh-number dependence of various contributions to the kinetic energy for the cases (a)  $Pr = 0.7$  and (b)  $Pr = 7$ , where diamonds, triangles, plus signs and crosses represent poloidal, toroidal, symmetric mean flow and antisymmetric mean flow energies as fractions of the total kinetic energy  $E_{kin}$ . For reference  $10^{-4}Ra/E_{kin}$  is shown by the stars. The aspect ratio is  $\Gamma = 10$  in all cases.

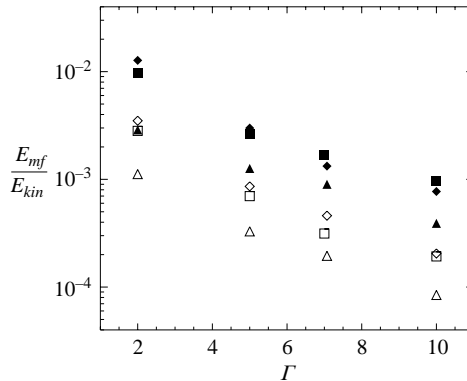


FIGURE 8. Aspect-ratio dependence of mean flow energies for  $Pr = 0.7$  (diamonds) and  $Pr = 7$  (triangles), both at  $Ra = 10^6$ , and for the case  $Pr = 0.7$ ,  $Ra = 10^7$  (squares). Open and filled symbols denote the kinetic energy of the symmetric and antisymmetric parts of the mean flow, again as fractions of the total kinetic energy.

of the velocity field changes with  $Ra$  in the case  $Pr = 0.7$ . Only the energy fractions of the toroidal component and of the antisymmetric mean flow increase slightly with  $Ra$ . In the case  $Pr = 7$ , the energies of the mean flow and of the toroidal component of the velocity field are rather minute at low values of  $Ra$ ; but they increase fairly rapidly such that they approach for  $Ra = 10^6$  the values found in the case  $Pr = 0.7$ .

It must be kept in mind that the mean flow is strongly dependent on the aspect ratio  $\Gamma$ . In fact, it must be expected that the mean flow vanishes in the limit of infinite aspect ratio since, in that limit, the mean flows generated by convection patches of all possible orientations tend to be averaged out. The mean flow as discussed in this section reflects in that limit the properties of large-scale horizontal motions. The time dependence and the symmetry with respect to the mid-plane of the layer of the mean flows studied in low-aspect-ratio cases are thus of general importance. Some results on the aspect ratio dependence are provided by figure 8. It would be of interest to

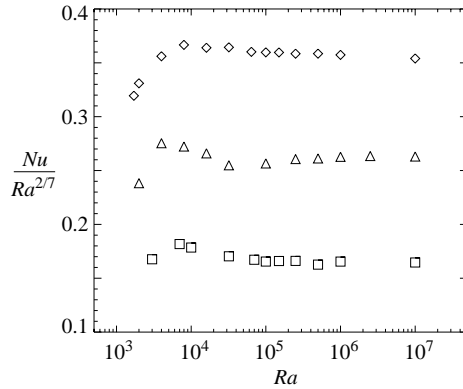


FIGURE 9. Nusselt number as a function of Rayleigh number for  $\Gamma = 10$  and  $Pr = 0.7$  (diamonds),  $Pr = 7$  (triangles) and  $Pr = 30$  (squares). Values shown for  $Pr = 0.7$  and  $Pr = 7$  are shifted by  $+0.2$  and  $+0.1$ , respectively.

proceed beyond the limit of  $\Gamma = 10$  at  $Ra = 10^7$  in order to understand better the spectral properties of large-scale motions induced by convection, but because of the present limits of computer capacity, this task has to be postponed for future studies.

Before closing this section we wish to mention that two-dimensional mechanisms of mean flow generation by convection rolls have been considered for a long time. For an early review see Busse (1983). Motivated by the observations of mean flows in their experiment (Krishnamurti & Howard 1981), Howard & Krishnamurti (1986) developed a simple theory. Owing to a small initial tilt, convection rolls generate a mean shear which in turn enhances the tilt. This instability mechanism is the same as that analysed for forced convection rolls by Busse (1972) or as the mean-flow instability in the rotating annulus system (Busse 1983, 1986). In the case of non-rotating Rayleigh–Bénard convection, however, it has always been found (Bolton *et al.* 1986) that the mean flow instability envisaged by Howard & Krishnamurti (1986) is preceded by transitions from two-dimensional to three-dimensional convection. This is consistent with the result that large-amplitude mean flows as observed by Krishnamurti & Howard (1981) have not been found in the present simulations.

## 5. Heat transport by convection

The efficiency of the convective heat transport is commonly measured by the Nusselt number which is defined as the ratio of the heat transports with and without convection. Results for the Nusselt number  $Nu$  as a function of  $Ra$  are shown in figure 9. It appears that for the regime of Rayleigh numbers  $10^5 < Ra < 10^7$ , the power-law dependence  $Nu \sim Ra^{2/7}$  provides a good fit for the numerical data. Although this power law has been discussed in the literature for a while, we have used it here only for convenience and because it has been used before for representing experimental as well as numerical data. For a recent discussion of scalings, see Grossmann & Lohse (2000, 2001). The results of figure 9 agree quite well with the relationship  $Nu = 0.186Ra^{0.276}$  found by Kerr (1996) for  $Pr = 0.7$  and for a similar regime of Rayleigh numbers. Additional computed values of the Nusselt number for different values of  $Pr$  are presented in Kerr & Herring (2000). It is worth noting that these authors also find that  $Nu$  is lower by about 7% for air ( $Pr = 0.7$ ) than for water ( $Pr = 7$ ) at  $Ra = 10^7$ , as can be seen from figure 9. For higher Prandtl numbers, the

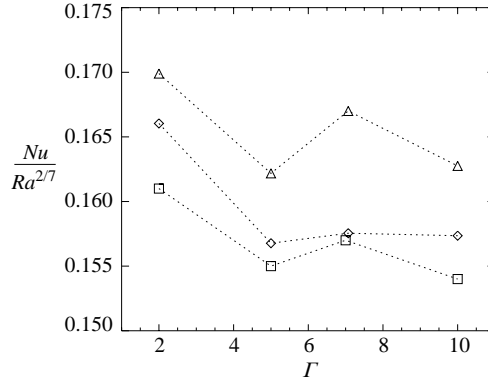


FIGURE 10. Dependence of the Nusselt number on the aspect ratio  $\Gamma$ . The three cases shown are for  $Ra = 10^6$ ,  $Pr = 0.7$  (diamonds) and  $Pr = 7$  (triangles), and  $Ra = 10^7$ ,  $Pr = 0.7$  (squares).

dependence of  $Nu$  on  $Pr$  seems to disappear since no significant difference between the values at  $Pr = 7$  and  $Pr = 30$  can be discerned.

Of particular interest is the dependence of the heat transport on the aspect ratio. Small aspect ratios favour the vertical component of the velocity field relative to the horizontal components and thus tend to enhance the heat transport. This effect is seen in figure 10, at least for  $\Gamma < 5$ . For larger values of  $\Gamma$ , no systematic dependence can be discerned, but the fact that the Nusselt number assumes maxima for certain values of the aspect ratio does not necessarily reflect insufficient numerical convergence. It is more likely that certain aspect ratios provide an especially good fit for the arrangement of convection rolls.

The effectiveness of the convective heat transport is mainly limited by processes in the thermal layers at the horizontal boundaries. Regions of high  $|\partial\Theta/\partial z|$  at  $z = 0, 1$  provide strong heat transfers between fluid and boundary, while regions of low  $|\partial\Theta/\partial z|$  correspond to larger thicknesses  $\delta$  of the thermal boundary layers and are thus prone to buoyancy-driven instabilities since the local Rayleigh number corresponding to  $Ra\delta^3/2$  is likely to exceed a critical value. According to the criterion of Busse (1967), the thermal boundary becomes unstable when the quantity  $NuRa^{-1/3}$  decreases with increasing  $Ra$  as is always the case in the considered Rayleigh-number regime according to the heat transport results of figure 10. It is of interest to compare the regions of high and low  $|\partial\Theta/\partial z|$  through a plot of the quantity

$$\left\langle \frac{\partial\Theta/\partial z - \langle \partial\Theta/\partial z \rangle}{|\partial\Theta/\partial z - \langle \partial\Theta/\partial z \rangle|} \right\rangle \text{ at } z=0 \tag{5.1}$$

as a function of  $Ra$  and  $Pr$ , as has been done in figure 11. In (5.1) the angular brackets indicate the average over the  $(x, y)$ -plane as well as over time. Positive values of the quantity (5.1) indicate that the regions of small  $|\partial\Theta/\partial z|$  exceed the regions of high  $|\partial\Theta/\partial z|$  since  $\partial\Theta/\partial z$  is always negative at the boundaries. Since high values of  $|\partial\Theta/\partial z|$  at the boundaries are usually caused by strong flows towards the respective boundary region, we expect a positive (negative) correlation of expression (5.1) with the quantity  $\langle v_z/|v_z| \rangle$  close to  $z = 0$  ( $z = 1$ ). Such a correlation appears to be realized at high values of  $Ra$  in the cases  $Pr = 0.7$  and  $Pr = 30$ , according to figure 12. In the case  $Pr = 7$ , the situation is less clear because the function  $\langle v_z/|v_z| \rangle$  is not even antisymmetric in  $z$  at the intermediate Rayleigh numbers of the order  $10^4$  to  $10^5$

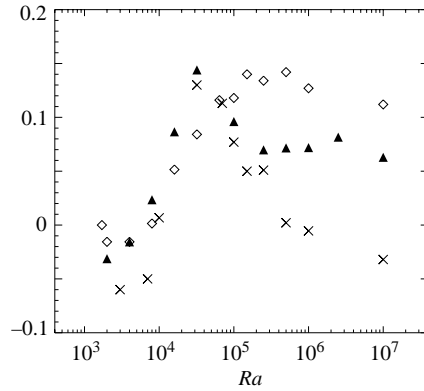


FIGURE 11. Rayleigh-number dependence of quantity (5.1) for  $\Gamma = 10$  and  $Pr = 0.7$  (diamonds),  $Pr = 7$  (triangles) and  $Pr = 30$  (crosses).

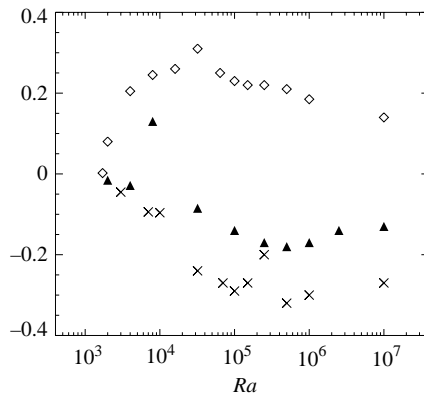


FIGURE 12.  $Ra$ -dependence of the quantity  $\langle v_z/|v_z| \rangle$  close to the lower boundary for  $\Gamma = 10$  and  $Pr = 0.7$  (diamonds),  $Pr = 7$  (triangles) and  $Pr = 30$  (crosses).

where convection in the form of asymmetric square cells appears to be dominant, according to the patterns shown in figure 3.

The dependence on  $z$  of the quantity  $\langle v_z/|v_z| \rangle$  reveals a persistent and, for turbulent convection, unexpected distinction between the dynamics at high and low values of the Prandtl number, as is evident from figure 13. While for values of  $Pr$  of the order unity or less the distribution of high and of low values of  $|v_z|$  appears to be dominated by plumes impinging with relatively high velocities onto the boundaries, a different situation is found for Prandtl numbers of order 7 and higher. Here, large values of  $|v_z|$  are associated with thermals moving away from the boundary. This distinction is well known for laminar convection rolls at low Rayleigh numbers as discussed, for example, in Busse (1989). This effect is indicated by the curves shown in figure 13 which reflect the inclination of the elliptical streamlines of the rolls towards the vertical symmetry plane of rising (descending) motion for low (high) values of  $Pr$  which causes the corresponding concentration of rising (descending) flow in the upper (lower) half of the layer. It is surprising that this distinction between high  $Pr$  and low  $Pr$  rolls found at low values of  $Ra$  persists close to the boundaries far into the turbulent regime. It thus represents another indication that convection in the thermal boundary layers reflects properties of convection in the entire layer at corresponding lower values of  $Ra$ .

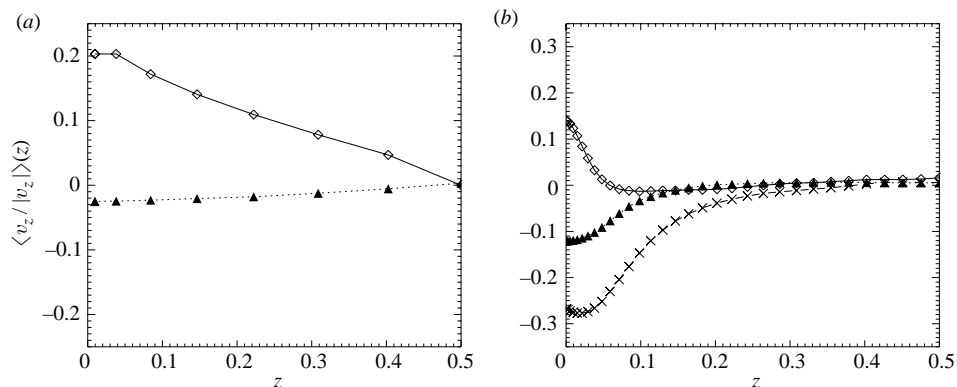


FIGURE 13. Time-averaged profiles of  $\langle v_z/|v_z| \rangle(z)$  for (a)  $Ra = 4 \times 10^3$  and (b)  $Ra = 10^7$ . Diamonds, triangles and crosses represent Prandtl numbers  $Pr = 0.7, 7$  and  $30$ . Again,  $\Gamma = 10$ .

## 6. Concluding remarks

The numerical simulations presented in this paper have covered only a limited range of Rayleigh and Prandtl numbers. Since the goal has been to simulate convection in large-aspect-ratio layers, it was felt that the horizontal periodicity interval should be chosen sufficiently large to allow for at least two roll pairs to be realized. Even though the computations have been carried out to values of  $Ra$  up to  $10^7$ , the dynamical processes found at these high Rayleigh numbers still reflect the processes introduced by the instabilities of rolls at values of  $Ra$  of the order of  $10^4$  to  $10^5$ . In particular, the properties of large-scale horizontal flows can be understood on this basis.

The dynamics of high-Rayleigh-number convection is governed primarily by the properties of the thermal boundary layers. The similarity of the secondary convection processes in these layers with convection in the entire layer at lower Rayleigh numbers suggests the beginning of an evolution towards a hierarchy of boundary layers as  $Ra$  tends to infinity. Very high Rayleigh numbers are accessible only in experimental investigations because of the limited numerical resolution that is affordable on currently available computers. Detailed measurements of properties of the thermal boundary layers require large dimensions of the experimental apparatus such as those of the convection chamber that has become available as the ‘Barrel of Ilmenau’ with its height of 7 m (Resagk *et al.* 2002). It is hoped that it will be possible to achieve a detailed contact between the results of this and other experiments in the case of moderate to large aspect ratios and the simulations reported in this paper.

The support of the Deutsche Forschungsgemeinschaft for the research reported in this paper is gratefully acknowledged.

## REFERENCES

- ASSENHEIMER, M. & STEINBERG, V. 1996 Observations of coexisting up- and downflow hexagons in Boussinesq Rayleigh–Bénard convection. *Phys. Rev. Lett.* **76**, 756–759.
- BALACHANDAR, S., YUEN, D. A. & REUTELER, D. M. 1996 High Rayleigh number convection at infinite Prandtl number with temperature-dependent viscosity. *Geophys. Astrophys. Fluid Dyn.* **83**, 79–117.
- BOLTON, E. W., BUSSE, F. H. & CLEVER, R. M. 1986 Oscillatory instabilities of convection rolls at intermediate Prandtl numbers. *J. Fluid Mech.* **164**, 469–485.

- BUSSE, F. H. 1967 On the stability of two-dimensional convection in a layer heated from below. *J. Math. Phys.* **46**, 140–150.
- BUSSE, F. H. 1972 On the mean flow induced by a thermal wave. *J. Atmosph. Sci.* **29**, 1423–1429.
- BUSSE, F. H. 1983 Generation of mean flows by thermal convection. *Physica* **9D**, 287–299.
- BUSSE, F. H. 1986 Asymptotic theory of convection in a rotating cylindrical annulus. *J. Fluid Mech.* **173**, 545–556.
- BUSSE, F. H. 1989 Fundamentals of thermal convection. In *Mantle Convection, Plate Tectonics and Global Dynamics* (ed. W. R. Peltier). Gordon and Breach, New York.
- BUSSE, F. H. & WHITEHEAD, J. A. 1971 Instabilities of convection rolls in a high Prandtl number fluid. *J. Fluid Mech.* **47**, 305–320.
- BUSSE, F. H. & WHITEHEAD, J. A. 1974 Oscillatory and collective instabilities in large Prandtl number convection. *J. Fluid Mech.* **66**, 67–79.
- CLEVER, R. M. & BUSSE, F. H. 1974 Transition to time-dependent convection. *J. Fluid Mech.* **65**, 625–645.
- CLEVER, R. M. & BUSSE, F. H. 1987 Nonlinear oscillatory convection. *J. Fluid Mech.* **176**, 403–417.
- CLEVER, R. M. & BUSSE, F. H. 1989 Nonlinear oscillatory convection in the presence of a vertical magnetic field. *J. Fluid Mech.* **201**, 507–523.
- CLEVER, R. M. & BUSSE, F. H. 1994 Steady and oscillatory bimodal convection. *J. Fluid Mech.* **271**, 103–118.
- CLEVER, R. M. & BUSSE, F. H. 1995 Standing and travelling oscillatory blob convection. *J. Fluid Mech.* **297**, 255–273.
- CLEVER, R. M. & BUSSE, F. H. 1996 Hexagonal convection cells under condition of vertical symmetry. *Phys. Rev. E* **53**, R2037–R2040.
- FRICK, H., BUSSE, F. H. & CLEVER, R. M. 1983 Steady three-dimensional convection at high Prandtl number. *J. Fluid Mech.* **127**, 141–153.
- GROSSMANN, S. & LOHSE, D. 2000 Scaling in thermal convection: a unifying theory. *J. Fluid Mech.* **407**, 27–56.
- GROSSMANN, S. & LOHSE, D. 2001 Thermal convection for large Prandtl numbers. *Phys. Rev. Lett.* **86**, 3316–3319.
- HARTLEP, T. & TILGNER, A. 2003 Rayleigh–Bénard convection at large aspect ratios. In *High Performance Computing in Science and Engineering '03*, pp. 343–357. Springer.
- HARTLEP, T., TILGNER, A. & BUSSE, F. H. 2003 Large scale structures in Rayleigh–Bénard convection at high Rayleigh numbers. *Phys. Rev. Lett.* **91**, 064501.
- HOWARD, L. N. & KRISHNAMURTI, R. 1986 Large-scale flow in turbulent convection—a mathematical model. *J. Fluid Mech.* **170**, 385–410.
- KERR, R. M. 1996 Rayleigh number scaling in numerical convection. *J. Fluid Mech.* **310**, 139–179.
- KERR, R. M. & HERRING, J. R. 2000 Prandtl number dependence of Nusselt number in direct numerical simulations. *J. Fluid Mech.* **419**, 325–344.
- KRISHNAMURTI, R. & HOWARD, L. N. 1981 Large scale flow generation in turbulent convection. *Proc. Natl Acad. Sci. USA* **78**, 1981–1985.
- LIPPS, F. B. 1976 Numerical simulation of three-dimensional Bénard convection in air. *J. Fluid Mech.* **75**, 113–148.
- MOSER, R. D., MOIN, P. & LEONARD, A. 1983 A spectral numerical method for the Navier–Stokes equations with application to Taylor–Couette flow. *J. Comput. Phys.* **54**, 524–544.
- RESAGK, C., BUSSE, F. H., DU PUIITS, R., THESS, A. & TILGNER, A. 2002 The barrel of Ilmenau: a novel facility for experiments on high Rayleigh number convection. In *Advances in Turbulence IX, Proc. 9th European Turbulence Conference, Southampton, 2002*. CIMNE, Barcelona.
- WILLIS, G. E., DEARDORFF, J. W. & SOMERVILLE, R. C. 1972 Roll-diameter dependence in Rayleigh convection and its effect upon the heat flux. *J. Fluid Mech.* **54**, 351–367.